# Transition from isometric to stretching ridges in thin elastic films

J. F. Fuentealba, O. Albarrán, E. Hamm, and E. Cerda
*Departamento de Física, Universidad de Santiago, Avenida Ecuador 3493, Estación Central, Santiago, Chile*
(Received 23 November 2014; revised manuscript received 20 February 2015; published 11 March 2015)

Isometric deformations in thin elastic films easily form ridges to connect large flat regions or facets. Depending on the forces applied or the boundary conditions imposed, these ridges can be isometric, with no stretching or "stretching ridges" when bending and stretching are required to relax the elastic energy. Here we study a simple configuration to observe the transition between an isometric ridge to the well-known stretching ridge observed in crumpled films, and obtain the parameters that determine the ridge type. Specifically, we show that the transversal size of a stretching ridge acts as a cutoff length scale: a ridge is isometric if its width is greater than this characteristic length.

DOI: 10.1103/PhysRevE.91.032407 PACS number(s): 46.50.+a, 46.32.+x, 46.05.+b, 46.25.−y

## I. INTRODUCTION

When twisting an elastic ribbon, pulling a flap from a film to tear it, or crumpling a film, we observe regions of high curvature where most of the energy is localized (see Fig. 1). Since the seminal work of Witten and Li [1], several works have extensively studied the nature of these ridges in crumpled structures and concluded that they account for most of the energetic cost at low confinement [2–7]. Ridges in a fully developed crumpled structure have a characteristic width given by $h \sim t^{1/3}W^{2/3}$, where $t$ is thickness and $W$ is the distance between the two ends of the ridge, or the length of the ridge. These ridges are saddle-shaped [see Fig. 1(a)] and are computed by a combination of bending and stretching. In contrast to these fully "developed" stretching ridges, isometric shapes can also show isometric ridges. The pulling and twisting of a ribbon, as studied in Refs. [8,9], can continuously increase the density of generators leading to ridges connecting two flat regions with no stretching [see Fig. 1(b)]. The size of these ridges, in an early stage of deformation, does not follow the scaling laws of a stretching ridge and is related to the levels of torque and force applied to the ends of the ribbon.

To connect these two types of ridges, Witten elegantly showed in Ref. [5] that truncating and rounding the ends of a ridge in a crumpled structure relaxes its curvature and the ridge becomes more isometric. Thus, the imposed curvature at the ends of the ridge controls its shape. A similar transition is observed when pulling a flap from a film constrained at its boundaries when it is being torn [10–15] [see Fig. 1(c)]. For relatively small forces, the strip looks cylindrical, with parallel generators perpendicular to the direction of pulling, and the whole shape is isometric. The ridge width can be easily computed by using the classical Euler's *Elastica*, which minimizes pure bending deformation. It gives $h_C = 2\sqrt{WB/F}$, [12,13] where $F$ is the force applied at the end of the strip, and $B$ is the bending stiffness of the film. As force is increased (and tearing is prevented), the ridge starts to develop a saddle shape, a clear sign of stretching, and therefore it is not isometric. Here we study this configuration experimentally and show that the ridge can be in two asymptotic states: a cylindrical isometric shape described by the *Elastica* (small force) or a nonisometric structure that responds to the scaling laws of a stretching ridge (large force).

## II. EXPERIMENTAL SETUP AND MEASUREMENTS

We attached polypropylene films (BOPP Innovia) with thicknesses of $t = 30$, 50, and 90 $\mu$m to a rectangular frame, and cut them into strips of $L \approx 0.94$ m in length in order to pull the films far from the position of the ridge. Since our films came coiled in a tube, we laid them flat on a horizontal table for at least one day before conducting the experiment. In every experiment we cut strips perpendicular to the direction of the coil in the tube to reduce the effects of natural curvature on our samples. As well, we used the outer side of the coiled film to face the optical system described below. The films were fairly isotropic, with a difference in Young's modulus of no more than 8% between the direction of coiling and its perpendicular direction, the second being the stiffer. The bending stiffnesses measured, along the orientation of bending in the experiments, were $B = 0.6 \times 10^{-5}$, $3 \times 10^{-5}$, and $15 \times 10^{-5}$ Nm, for the $t = 30$-, 50-, and 90-$\mu$m films, respectively. It was possible to adjust the frame width continuously to a range of $2\,\text{cm} < W < 20\,\text{cm}$ to obtain good variation in ridge lengths. The films were fixed to the frame with double-sided bonding tape and the flaps were notched at the position of the cracks with a 2-mm-diameter hole-puncher to avoid tearing during the experiment. The strips were pulled at 180 degrees from the plane of the film, which was aligned vertically in order to control gravity effects. Displacement at the pulling end was controlled by a stepper motor that moved at a fixed speed of 0.01 mm/s and a Futek force sensor was attached to the pulling point to track the force. An optical system was mounted to measure the curvature $R$ along the ridge. To measure the maximum width of the ridge $h$ we used a mirror placed below the ridge, oriented at 45 degrees from the direction of pulling (see Fig. 2). The area near the ridge was painted white to increase the contrast of the images [16].

Typical experimental curves for the transversal width $h$ are given in Fig. 3. The ridge shape was symmetrical with respect to the plane $y$-$z$ and its width decayed with the force until a plateau was reached where the ridge geometry changes slightly with the force ($h \sim F^{-\alpha}$, with $\alpha \lesssim 0.1$). With a further increase in the force the ridge became asymmetrical and the strip as a whole was stretched. We managed to pull the samples up to a maximum force of $F \lesssim 2$ kgf, at which point fracture was unavoidable given the small size of the notches used. The size of the ridge in this slightly varying region was

 

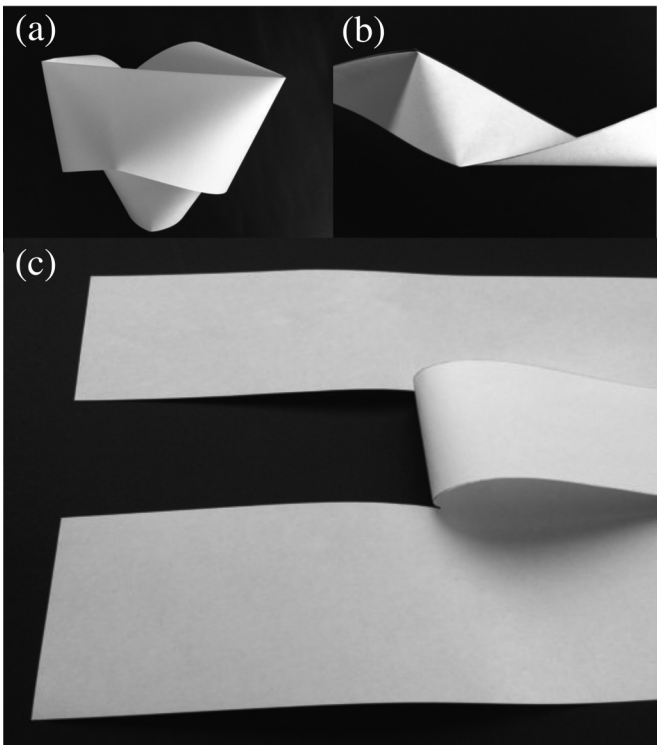


FIG. 1. Different configurations where a ridge emerges. (a) Pinching a sheet at two ends produces the classical saddle shape characteristic of a stretching ridge. (b) When stretching and twisting are applied to an elastic ribbon the shape can be described as flat facets connected by ridges. (c) Tearing a sheet by pulling a flap produces a narrow region of high curvature.

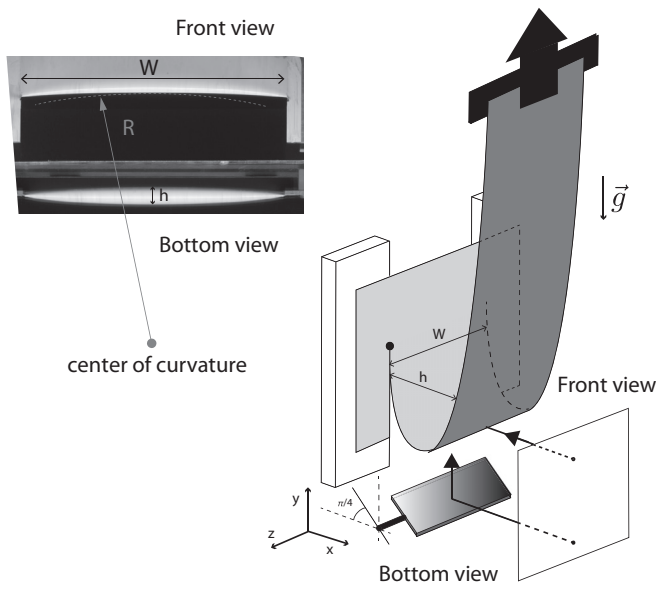


FIG. 2. Setup description. A film with a flap is attached to a framework and pulled along the vertical direction. The optical system in front of the system captures the geometry of the ridge. The camera view shown in the inset gives the shape of the ridge when pulling is applied. The length of the ridge $W$, its width $h$, and the longitudinal curvature $R$ are defined in the figure.

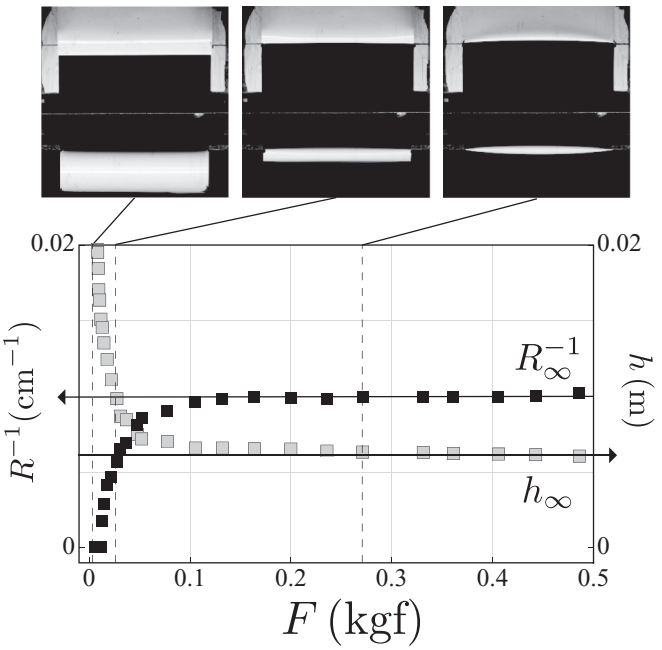


FIG. 3. A typical experimental curve for $t = 50\,\mu$m and $W = 10$ cm, where the ridge size $h$ (gray squares, right ordinate axis) and longitudinal curvature $1/R$ (black squares, left ordinate axis) are tracked as force (in kilogram force) is increased. These variables are very sensitive to the force when gently pulling and reach the values $h_\infty$ and $1/R_\infty$ for $F \approx 0.5$ kgf. The insets show photographs of the ridge (front and bottom view) shape for specific values of the force.

defined as $h = h_\infty$ for $F \approx 0.5$ kgf, a force where the ridge shape remained symmetrical throughout our experiments. Similarly, the longitudinal curvature $1/R$ increased from zero to a constant value $1/R_\infty$, showing that the ridge bends in the longitudinal direction for large forces. We show in the following sections that the rapid change in ridge geometry with force is explained by assuming a cylindrical ridge and modeling its deformation with the *Elastica*. Contrastingly, the asymptotic state is a static structure that follows the scaling laws of a stretching ridge. We finally show that the transition reveals the competition between these two solutions to relax the elastic energy in the ridge.

## III. CYLINDRICAL RIDGE

Since for small forces the ridge is cylindrical (see Fig. 2), we expect that its shape can be explained by using the *Elastica* (see Appendix) with one boundary clamped at $s = 0$, the other end at $s = L$, and a constant vertical force applied $F\hat{y}$. The analysis is very simple if gravity is neglected: the size of the ridge must be given by $h = h_C$. Thus, size decays with force according to the power law $h \sim F^{-1/2}$ with the force. However, because the applied force is small at the beginning of the experiment, gravity and the total length $L$ of the system play an important role in describing the size of the ridge. We define the dimensionless applied force $f = FL^2/BW$ and the dimensionless mass $m = MgL^2/BW$, where $M$ is the total mass of the film, so that the ridge size must be given by a dimensionless relation $h/L = \Pi(f,m)$. Note that the dimensionless mass does not depend on the width $W$ of

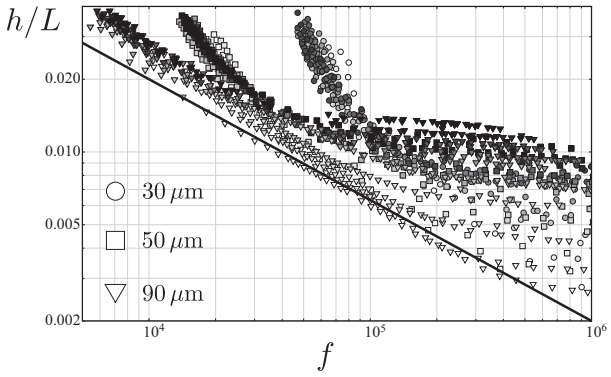


FIG. 4. Log-log showing $h$ as a function of the force applied for three different values of thickness. The solid line corresponds to the cylindrical approximation $h_C/L = 2/\sqrt{f}$ obtained for $m = 0$. The large amount of data for each thickness corresponds to experiments with different values of ridge length $W$ increasing from 2 to 20 cm in intervals of 1 cm. The gray scale shows the ridge length: darker values corresponding to larger values of $W$.

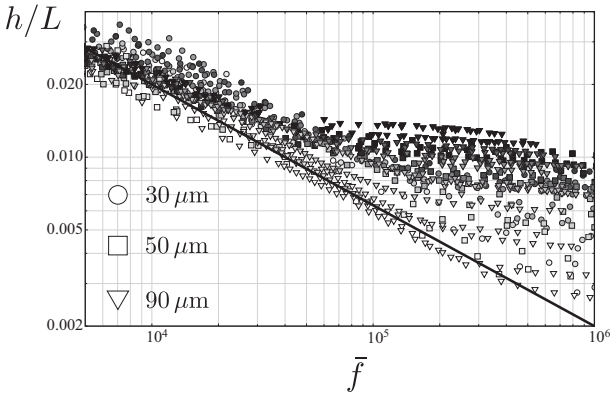


FIG. 5. Data corrected by using the dimensionless mass measured for each sample. The solid line corresponds to the approximation $h_C/L = 2/\sqrt{\bar{f}}$, where $\bar{f} = f - m$.

our strips, so that for experiments with a fixed length $L$, the parameter varies only because of thickness. Unexpectedly, the effect of mass becomes more important for thinner films since $m \sim t^{-2}$ for an isotropic material where $B = Yt^2/12(1-\nu^2)$ [17]. Here $Y$ is the two-dimensional Young modulus and $\nu$ the Poisson ratio of the film. Figure 4 shows that thinner films depart more from the value $h = h_C$. Thus, for a given dimensionless force $f$, the ridge width is greater for thinner films since weight is relevant and counterbalances the pulling force in our setup.

The data for a small force in Fig. 4 falls into three different groups that are related to the three thicknesses used in our experiments. However, the range in the results for a small force in each group is greater for thinner films, showing that small variations in the dimensionless mass (like the paint we used near the ridge to visualize its geometry) can have an important effect on the data. To correct these variations we weighed the samples after each experiment and computed their dimensionless mass $m$. For example, for the films of ridge length $W = 20$ cm and thicknesses of $t = 30$, 50, and 90 $\mu$m, we measured $m \approx 4.3 \times 10^4, 1.3 \times 10^4, 4.7 \times 10^3$, respectively. We expected that the first correction to the effect of the weight would be captured by the translation $f \to \bar{f} = (f - m)$ for small values of $m$. Here, $\bar{f}$ is the effective pulling force, so that the force decreases by $m$. Accordingly, the size of the ridge is given by the corrected formula $h_C/L = 2/\sqrt{\bar{f}}$. Figure 5 shows that the data can be collapsed for small forces by using the effective force $\bar{f}$. The remaining variation in the data for a small force is explained by a second regime observed when $f \approx m$. In that case, the pulling force is so small that it just balances gravity, and the ridge size is dictated by the elastogravity length $\ell_g = (BWL/Mg)^{1/3}$ [18]. A more precise analysis of the *Elastica* containing this gravity dominated regime is given in the Appendix.

For large forces, the prediction obtained with the *Elastica* approximation is no longer valid. As we show in Fig. 3, the ridge width reaches an asymptotic state that cannot be captured by the cylindrical approximation, which is a monotonically decreasing function of force.

## IV. STRETCHING RIDGE

We now analyze the asymptotic state obtained for a large force and recognize it as a stretching ridge. Stretching ridges have been intensively studied and described in Refs. [1–4]; however, we are not aware of any experimental work studying their characteristic scaling laws even though stretching ridges were first reported in the mid-1990s. The main geometrical results for the ridge are given for the two radii of curvature $R^{\parallel}$ and $R^{\perp}$, longitudinal and transversal to the ridge. For a stretching ridge $R^{\parallel} \sim t^{-1/3}W^{4/3}$ and $R^{\perp} \sim t^{1/3}W^{2/3}$; hence, the inverse of the Gaussian curvature at the center of the ridge, strikingly, does not depend on thickness and scales like $(R^{\parallel}R^{\perp}) \sim W^2$ (negative).

We have direct access to the longitudinal curvature of the ridge in our experiment because $R_\infty \approx R^{\parallel}$ and we expect the width of the ridge to be proportional to the transversal curvature, or $h_\infty \approx 2R^{\perp}$. Therefore, we can check if the ridge becomes a stretching ridge by studying these two length scales for a large force as a function of the length $W$ and thickness $t$. Figure 6 shows the transversal and longitudinal curvatures for different values of ridge length and thickness. More importantly, the range of values of ridge width observed in Fig. 5 for large forces can be understood by using the scaling laws of a stretching ridge. The transversal and longitudinal radii of curvature can be made to collapse to the relations $h_\infty \approx 0.78\, t^{1/3}W^{2/3}$ and $R_\infty \approx 0.83\, t^{-1/3}W^{4/3}$. And the inverse of the Gaussian curvature follows even more closely the scaling predicted for a stretching ridge $h_\infty R_\infty \approx 0.65\, W^2$ (see Fig. 6 inset).

Note that the von Kármán number $W/t$ in our experiments covers the range $[222 < W/t < 6666]$, which includes smaller values than the range $3000 < W/t$, where previous numerical works [3,19] predicted the scaling laws for a stretching ridge to emerge [20]. However, the same authors have made clear that this range is sensitive to the specific configuration in which a ridge is studied.

Although the prefactors for the scalings describing the geometry of a stretching ridge are not universal, we can

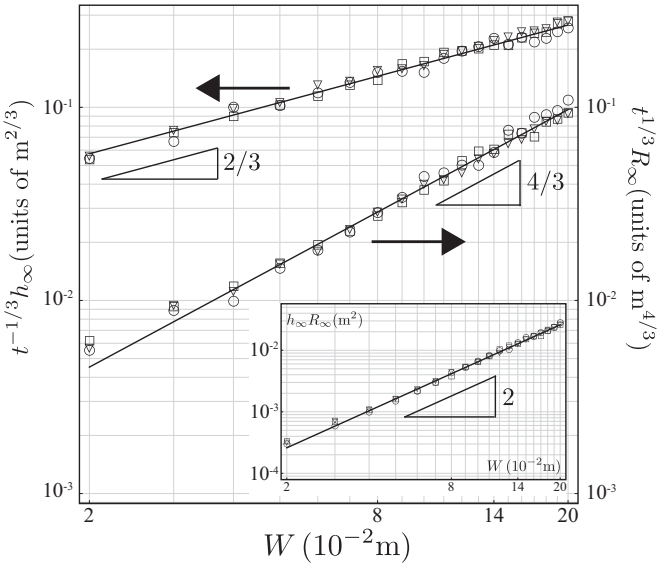


FIG. 6. Log-log showing the experimental values of $h_\infty$ (left ordinate axis) and $R_\infty$ (right ordinate axis) as a function of $W$ for three thicknesses $t = 30\,\mu$m (◯), 50 $\mu$m (□), and 90 $\mu$m (▽). These values are made to collapse by using the scaling laws of a stretching ridge: the solid lines correspond to the fits $t^{-1/3}h_\infty \approx 0.78\,W^{2/3}$ and $t^{1/3}R_\infty \approx 0.83\,W^{4/3}$. Inset: The inverse of the Gaussian curvature for the asymptotic state, $h_\infty R_\infty$, as a function of the ridge width. The solid line follows the scaling $h_\infty R_\infty \approx 0.65\,W^2$.

compare the experimental results with the numerical scaling for the transversal curvature provided in Ref. [3]. For a rectangular strip bent by normal forces it is obtained $W/R^\perp \approx 0.4\,\alpha^{4/3}\lambda^{-1/3}$, where $\lambda = (B/Y)^{1/2}/W$ [21]. Here $\pi - 2\alpha$ gives the "dihedral angle" or the angle between the two flat planes defining the ridge. Since for our system $\alpha = \pi/2$ and $\nu \approx 1/3$, the numerical scaling predicts the relation $h_\infty \approx 1.8\,t^{1/3}W^{2/3}$, which falls above the scaling obtained from our experiments.

## V. THE TRANSITION

The ridge can be in one of two asymptotic states. However, the condition that transforms a cylindrical ridge into a stretching ridge is still not understood. A simple tabletop experiment proposed by Witten in Ref. [5] made by truncating and rounding the ends of a ridge to the radius of curvature $R_0$ shows that for $R_0 \sim R^\perp$ a stretching ridge relaxes to have parallel generators, hence stretching decreases. In our case we expected a similar transition to be obtained when the radius of curvature dictated by the *Elastica* approximation is of the same order as the size of the stretching ridge or $h_C \sim h_\infty$. Thus, if the size of the ridge given by the *Elastica*, $h_C$, is greater than that of a stretching ridge, the ridge will prefer to maximize its size (and minimize its curvature) to the value given by the isometric state. In contrast, if $h_C$ is smaller than the stretching ridge, the ridge will relax its energy (and minimize its curvature) by increasing its size in the middle to $h_\infty$.

The balance $h_C \sim h_\infty$ gives a critical force for the transition

$$F_* = 4\frac{BW}{h_\infty^2} = k\frac{B}{t^{2/3}W^{1/3}}, \qquad (1)$$

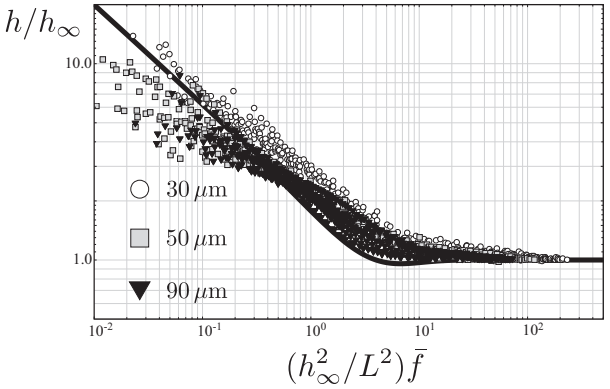


FIG. 7. The same data as described in the legend of Fig. 5 represented in the dimensionless variables suggested by the asymptotic behavior for small and large forces. The solid line corresponds to the fit $h/h_\infty = (2/\sqrt{x} - 1)e^{-x/4} + 1$, where $x = (h_\infty^2/L^2)\bar{f}$.

where $F_*$ is the effective pulling force and $k \approx 6.6$. Note that this is equivalent to assuming the general fit $h = [2L/\sqrt{\bar{f}} - h_\infty]e^{-\bar{f}/\bar{f}_*} + h_\infty$, with $\bar{f}_* = F_*L^2/BW$, which captures the asymptotic behavior for small and large forces [22]. Using the definition of the critical force, we obtain that the ridge width is given by the simple relation $h/h_\infty = (2/\sqrt{x} - 1)e^{-x/4} + 1$, where $x = (h_\infty^2/L^2)\bar{f}$. Figure 7 shows that the proposed fit works well for describing the transition from a cylindrical to a stretching ridge. Moreover, the figure shows the validity of the model fit. There is a slight departure of the data from the cylindrical approximation for a small force, which is due to the gravity dominated regime (see Appendix), and a decreasing $h$ is exposed in the large force limit because of the still varying ridge shape.

## VI. CONCLUSIONS

Relation Eq. (1) provides a useful way to know when an isometric description is no longer valid. Although it is obtained for the specific configuration given in Figs. 1(c) and 2, it rests on the general idea that the isometric approximation near a ridge is valid if the radius of curvature imposed by boundary conditions or forces is larger than the size of a stretching ridge. Thus, $h_\infty$, a length dictated by elasticity, acts as a cutoff length scale. Since this length increases with system size ($h_\infty \sim W^{2/3}$), or equivalently, the critical force decreases for larger values of $W$ ($F_* \sim W^{-1/3}$), it is reasonable to assume an isometric solution for smaller systems or smaller applied forces in a displacement- or force-controlled experiment, respectively.

Our results can be applied to understanding how energy is stored before tearing in a configuration as in Fig. 2. This observation is relevant for tearing experiments where the force is of the order $F \approx \gamma t$, where $\gamma$ is the work of fracture of the material. We expect to observe an isometric ridge for small samples ($F < F_*$) during tearing. Moreover, since $\ell_c = \gamma t/Y$ is similar to an elastocapillary length and has the order $\ell_c \approx 1\,\mu$m for typical polymer films [12,13], we predict the isometric approximation to be valid during tearing for a ridge length smaller than $W_* = t[p\,t/\ell_c]^3$, where $p = k/12(1-\nu^2) \approx 0.6$. It yields $W_* \approx 1.3$ m! for a packaging

film of $t = 50\,\mu$m. Therefore, the understanding of tearing of these films in practical applications must be made in the framework of isometrically deformed films. In this regard we are puzzled by recent works that explain tearing in thin films by using a stretching ridge to account for the elastic energy distribution during fracture [14,15,23].

An analytical approach connecting these two asymptotic states and describing the transition in an equivalent or similar configuration is much needed. Previous theoretical works studying stretching ridges have been made in the context of approximations of large deflection but with small slopes using the Föppl-von Kármán equations. However, here we have an example where the theoretical framework that accounts for large displacements in isometric deformations needs to be amended by a theory explaining the emergence of stretching ridges.

## ACKNOWLEDGMENTS

We are grateful to C. Santangelo and R. Schroll for many discussions. E.C. thanks the Physics Department of the Universidad de Buenos Aires for its hospitality during the final stages of this work. E.C. acknowledges the support of Fondecyt Project No. 1130579. E.H. acknowledges the support of Fondecyt Project No. 1140225.

## APPENDIX: THE ELASTICA APPROXIMATION

In the *Elastica* approximation the problem is reduced to solve the equilibrium equations [24]

$$\dot{\mathbf{T}} + \mathbf{K} = 0, \tag{A1}$$

$$\dot{\mathbf{M}} + \mathbf{t} \times \mathbf{T} = 0, \tag{A2}$$

where $\mathbf{K}$ is the external force per unit of line of the strip, $\mathbf{T}$ and $\mathbf{M}$ are the force and moment in the cross section, respectively, and $\mathbf{t}$ is the tangent to the centerline. We use the notation $(\dot{\cdot}) = d/ds(\cdot)$. For our problem $\mathbf{K} = -\sigma W g \hat{y}$, where $\sigma = M/WL$ is the density of mass per unit of area so that an integration of the first equation gives $\mathbf{T} = [F - \sigma W g(L-s)]\hat{y} - R\hat{x}$. Here $F$ and $R$ are the forces applied at the far end to keep the strip attached to the force sensor. Since we measure the vertical component of the force, the pulling force $F$ is known.

We use the Bernoulli-Euler relation between moments and curvature, $\mathbf{M} = BW\dot{\phi}\hat{z}$ [25], and the kinematic relation $\mathbf{t} = \sin\phi\hat{x} - \cos\phi\hat{y}$ (see Fig. 8) to obtain an equation for the angle $\phi$,

$$BW\ddot{\phi} + [F - \sigma W g(L-s)]\sin\phi - R\cos\phi = 0, \tag{A3}$$

where the position of the coordinates $(x, y)$ are given by

$$\dot{x} = \sin\phi \quad \dot{y} = -\cos\phi. \tag{A4}$$

Equations (A3) and (A4) have been extensively studied in Ref. [18] in connection with the problem of hair shape, so that here we limit our analysis to solving the equations numerically for the relevant boundary conditions (BCs) used in the experiment. The strip in our experiment was clamped at both ends, so then the appropriate BCs are $x = y = \phi|_{s=0} = 0$, $x|_{s=L} = 0$, and $\phi|_{s=L} = \pi$. Since we have 5 BCs, the fourth-order ODE gives the value of the unknown force $R$.

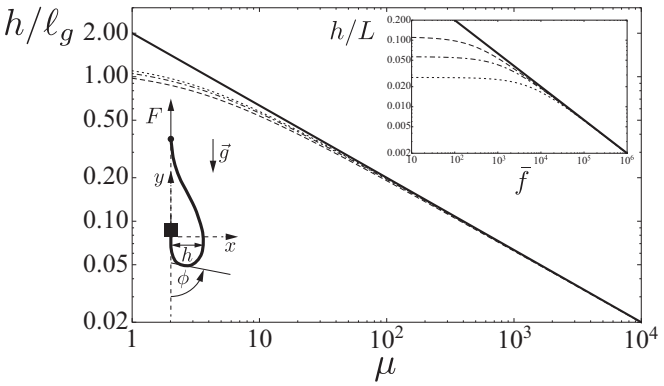


FIG. 8. Numerical simulation of Eqs. (A3) and (A4). Top inset shows the ridge size in the coordinates $\bar{f} - h/L$ used in Fig. 5. The dashed, dot-dashed, and dotted lines correspond to the dimensionless masses $m = 10^3, 10^4, 10^5$, respectively, that covers the relevant values used in our experiments. The main figure shows the collapse of the curves when using the coordinates $\mu - h/\ell_g$. The solid lines give the cylindrical approximation $h_C/L = 2/\sqrt{\bar{f}}$ and $h_C/\ell_g = 2/\sqrt{\mu}$ in both figures. The lower inset gives a schematic of the ridge shape projected in the plane $x$-$y$.

The scaling of the vertical and horizontal coordinates, and the arclength by the elastogravity length $\ell_g$ gives a simplified equation,

$$\ddot{\phi} + \frac{(f-m)}{m^{2/3}}\sin\phi + \bar{s}\sin\phi - k\cos\phi = 0, \tag{A5}$$

where $\bar{s} = s/\ell_g$ is the dimensionless arclength and $k \equiv RL^2/BW$, the eigenvalue, represents the unknown horizontal force. The scaling shows that an important dimensionless parameter is $\mu \equiv (f-m)/m^{2/3}$. However, the pulling end is at the position $\bar{s} = L/\ell_g = 1/m^{1/3}$ that adds a new dimensionless parameter to the problem. Since $\ell_g$ is of the order of centimeters (or less) in our films, we have $L \gg \ell_g$ or $m^{1/3} \gg 1$. It also shows that the exact BCs at the pulling position, or equivalently the parameter $m$ in this description, are not very important in the determination of the ridge size and we could expect a relation of the form $h/\ell_g = \Pi(\mu)$.

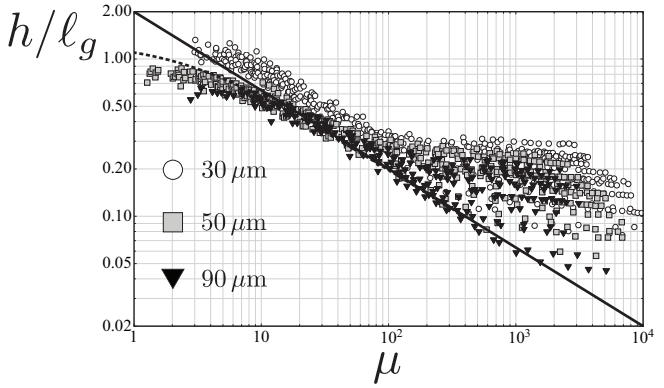


FIG. 9. The data in the dimensionless variables $\mu - h/\ell_g$. The dotted line corresponds to the numerical simulation for $m = 10^5$ and the solid line to the approximation $h_C/\ell_g = 2/\sqrt{\mu}$.

Figure 8 inset gives the ridge size in the coordinates $\bar{f} - h/L$ showing that the scaling $h_C/L = 2/\sqrt{\bar{f}}$ works well for large force but it is not correct for $f - m \approx 0$. The ridge sizes converge in that limit to different values depending on the specific value of $m$. The figure also shows that for the range $m \sim 10^3 - 10^5$ a crossover from the ridge size dominated by $h_C$ to the ridge size dictated by the elastogravity length must be observed when the parameter $\bar{f}$ is $\bar{f} \sim 10^3 - 10^4$. Therefore, we expect the data at the extreme left side of Fig. 5 to be in the crossover region. This explains also the separation from the cylindrical approximation of the data for small force in Fig. 7.

The numerical curves in Fig. 8 inset can be collapsed when using coordinates $\mu - h/\ell_g$ (see Fig. 8). It shows that the ridge size in the *Elastica* approximation is controlled by the dimensionless parameter $\mu$ for small and large force. Figure 9 shows the experimental data when using $\mu$ as parameter. The collapse is very good for small force and for the films of thicknesses $t = 50$ and 90 $\mu$m, but this is not the case for our 30-$\mu$m films. These films are more sensitive to variation in bending stiffness and nonuniform distribution of mass due to the painting process [16]. In fact, an increase of the bending stiffness to 30–40% makes the data for the 30-$\mu$m films approach the numerical curve of Fig. 9 for small force.


[1] T. A. Witten and H. Li, Europhys. Lett. **23**, 51 (1993).
[2] A. E. Lobkovsky, S. Gentes, H. Li, D. Morse, and T. A. Witten, Science **270**, 1482 (1995).
[3] A. E. Lobkovsky, Phys. Rev. E **53**, 3750 (1996).
[4] T. A. Witten, Rev. Mod. Phys. **79**, 643 (2007).
[5] T. A. Witten, J. Phys. Chem. B **113**, 3740 (2009).
[6] G. A. Vliegenhart and G. Gompper, Nat. Mater. **5**, 216 (2006).
[7] T. Tallinen *et al.*, Nature Phys. **8**, 25 (2009).
[8] A. P. Korte *et al.*, Proc. Roy. Soc. A **467**, 285 (2011).
[9] J. Chopin and A. Kudrolli, Phys. Rev. Lett. **111**, 174302 (2013).
[10] A. G. Atkins, Endeavour **18**, 2 (1994).
[11] A. G. Atkins, Science and Public Affairs, published by British Science Association, No. 19 (Autumn, 1994).
[12] E. Hamm *et al.*, Nat. Mat. **7**, 386 (2008).
[13] B. Roman, Int. J. Fract. Mech. **182**, 209 (2013).
[14] E. Bayart, A. Boudaoud, and M. Adda-Bedia, Phys. Rev. Lett. **106**, 194301 (2011).
[15] E. Bayart *et al.*, Eng. Fract. Mech. **77**, 1849 (2010).
[16] The painting produced an increase in the bending stiffness lower than 10% for the 50- and 90-$\mu$m films. However, an increase in almost 30% was observed for the 30-$\mu$m films, depending on curing time.
[17] E. H. Mansfield, *The Bending and Stretching of Plates* (Cambridge University Press, Cambridge, 1989).
[18] B. Audoly and Y. Pomeau, *Elasticity and Geometry: From Hair Curls to the Nonlinear Response of Shells* (Oxford University Press, Cambridge, 2010).
[19] A. E. Lobkovsky and T. A. Witten, Phys. Rev. E **55**, 1577 (1997).
[20] References [3, 19] use the dimensionless parameter $\lambda = \sqrt{B/Y}/W$ to describe the proximity to the stretching ridge asymptotics. For $\lambda < 10^{-4}$ the ridge can be characterized as a stretching ridge. This is equivalent to a von Kármán number in the range $3000 < W/t$.
[21] We use Fig. 7 of the cited article where the numerical scaling $W/R_\perp \approx 5.2\alpha^{4/3}$ is obtained for a ridge with $\lambda = 5 \times 10^{-4}$.
[22] The fit could be equivalently written as $h = [2L/\sqrt{\bar{f}} - h_\infty]g(\bar{f}/\bar{f}_*) + h_\infty$, where $g(x)$ is a function such that $g(x) \approx 1$ for $x < 1$ and $g(x) \approx 0$ for $x > 1$. The exponential is a simple choice.
[23] F. Brau, Phys. Rev. E **90**, 062406 (2014).
[24] L. D. Landau and E. M. Lifshitz, *Theory of Elasticity* (Butterworth-Heinemann, Oxford, 1998).
[25] E. Cerda and L. Mahadevan, Proc. R. Soc. A **461**, 671 (2004).